Electronic Supplementary Information (ESI)

Chaotropic Anion Based "Water-in-Salt" Electrolyte Realizes a High Voltage Zn–Graphite Dual-Ion Battery

Zahid Ali Zafar [a,b], Ghulam Abbas [b,c], Karel Knížek [d], Martin Silhavik [a], Prabhat Kumar [a], Petr Jiříček [e], Jana Houdková [e], Otakar Frank [c], Jiří Červenka [a,*]

[a] Department of Thin Films and Nanostructures, FZU - Institute of Physics of the Czech Academy of Sciences, Cukrovarnicka 10/112 162 00 Prague 6, Czech Republic

[b] Department of Physical Chemistry and Macromolecular Chemistry, Faculty of Science, Charles University in Prague, Hlavova 2030, 128 43 Prague 2, Czech Republic

[c] J. Heyrovsky Institute of Physical Chemistry of the Czech Academy of Sciences, Dolejskova 2155/3, 183 23 Prague 8, Czech Republic

[d] Department of Magnetics and Superconductors, FZU - Institute of Physics of the Czech Academy of Sciences, Cukrovarnicka 10/112 162 00 Prague 6, Czech Republic

[e] Department of Optical Materials, FZU - Institute of Physics of the Czech Academy of Sciences, Cukrovarnicka 10/112 162 00 Prague 6, Czech Republic

*Corresponding author, email: cervenka@fzu.cz

Experimental Section

Materials: $Zn(ClO_4)_2.6H_2O$ and Zn metal (99.98%, thickness-0.25 mm) were purchased from Alfa-Aesar. A graphite paper sheet (GP, >99%, thickness 0.2 mm) and polytetrafluoroethylene (PTFE)-treated hydrophobic carbon paper (120 Toray carbon paper) were acquired from Graphit Kropfmühl, GmbH, Germany, and Fuel Cell Store, USA, respectively. Whatman® GF/D glass microfiber filters were purchased from Mar-Con, s.r.o., Czech Republic.

Electrolyte Preparation: The supersaturated 8 *m* (mol/kg) or water-in-salt (WiS electrolyte) and dilute 0.5 *m* $Zn(ClO_4)_2$ aqueous electrolytes were prepared by mixing the respective quantities of $Zn(ClO_4)_2.6H_2O$ (Alfa-Aesar) and deionized water (conductivity < 0.26 μScm^{-1}) under continuous stirring. It was determined that on average there are 0.11 moles of Zn^{2+} per 1 mole of H_2O in the 8 *m* $Zn(ClO_4)_2$-WiS electrolyte, whereas there are only 0.009 moles of Zn^{2+} per 1 mole of H_2O in the dilute 0.5 *m* $Zn(ClO_4)_2$ electrolyte.

Fabrication of Zn-Graphite Dual-ion Batteries: The two-electrode Zn-graphite dual-ion batteries were fabricated by placing the $Zn(ClO_4)_2$ -WiS electrolyte impregnated GF/D glass microfiber separator in between a Zn anode and a binder-free GP cathode. Finally, the cell was enclosed and well-sealed in a plastic foil by using a heat sealer (Tefal VT254070 Vacupack classic). Before assembling the batteries, Zn foil was rinsed with acetone and the GP surface was peeled off by using a Kapton tape to enhance the active surface area and reduce the hydrophobicity of the GP (see Fig. 3 a, main text). The binder-free GP cathode had dimensions of 10 × 10 × 0.2 mm and an active mass density of ~18 mg cm^{-3}. The dimensions of the Zn anode were 15 × 15 x 0.25 mm. 400 µl of the as-prepared WiS electrolyte was used in the experiments.

Electrochemical Performance Measurements: The electrochemical stability window of the freshly prepared electrolytes was assessed on a glassy carbon electrode (W.E.) in a standard 3-electrode set-up, where platinum (Pt) was used as a counter electrode (C.E.) and Ag/AgCl pseudo-reference electrode (R.E.). The potential of the pseudo-reference electrode was calibrated to be 220 mV against the standard Ag/AgCl reference electrode with a 3 M KCl aqueous solution. The potentiostatic cyclic voltammetry (CV), linear sweep voltammetry (LSV), and electrochemical impedance spectroscopy (EIS) were performed by using a potentio/galvanostat (Metrohm Autolab PGSTAT302N) on the as-assembled 2-electrode type cells. The galvanostatic charge/discharge (GCD) and cycle life tests were carried out using a battery tester (Neware, China) at constant (dis)charging current densities at room temperature. The capacity was determined on the basis of the mass of the graphite paper, i.e. 18 mg cm^{-2}.

Characterization: A TESCAN scanning electron microscope (SEM) was used for the analysis of the surface morphology of the electrodes. *Operando* Raman spectroscopy was performed on the home-made electrochemical cells using a battery tester and a Renishaw Invia™ confocal Raman spectroscope equipped with an optical microscope, a He-Cd blue laser (442 nm excitation wavelength), and 2400 l/mm diffraction grating. *Operando* X-ray diffraction (XRD) was carried out on a Bruker D8 Advance X-ray diffractometer (λ = 1.54 Å, Cu-k α radiation). All the XRD measurements were collected in the 2Θ (theta) angles of the range of 10° to 60° with the step rate of 0.02° using a *Lynxeye* detector and applying an accelerating voltage of 40 kV and a current of 40 mA. The total XRD scan time was set to 10 min to deliver a sufficient resolution while performing *in-situ* (dis)charge of the Zn-graphite dual-ion batteries equipped with a top Kapton window. The chemical nature of the intercalation species in the electrodes was probed via X-ray photoelectron spectroscopy (XPS) by using an AXIS Supra photoelectron spectrometer (Kratos Analytical Ltd, UK) with a monochromated Al Kα (1486 eV) excitation source. To probe the bulk of the samples, the samples were sputtered using Ar ions. The Ar ion sputtering was carried out by a Minibeam 6 ion gun operating in a cluster mode with a raster area of 2 x 2 mm for 600 seconds. The Ar ion clusters were composed of roughly 1000 atoms with an ion energy of 5 keV. The base pressure during the XPS measurements was 2 x 10^{-8} torr. X-ray energy dispersive spectroscopy (EDS) was carried out on the samples using an electron probe microanalyzer JEOL JXA-8230 equipped with an energy dispersive spectrometer Bruker QUANTAX 200 with a data processing software Esprit 2.2.

Contact angle measurement: Wettability of pristine and surface modified GP electrodes with the WiS-electrolyte was assessed by the measurement of contact angle. A small droplet of the WiS-electrolyte was placed on the surface of electrodes while recording using a digital camera. Later, the contact angle was measured between the electrode-electrolyte interface by drawing tangents to the points of droplet curves which are simultaneously in contact with electrode, electrolyte and air.

Ionic conductivity measurement of $Zn(ClO_4)_2$ WiS-Electrolyte: Ionic conductivity of the $Zn(ClO_4)_2$ WiS-electrolyte was measured by employing electrochemical impedance spectroscopy (EIS) from 0.01 Hz To 100 kHz. Briefly, the electrolyte resistance (*Rs*) was measured in an electrolytic tank with two symmetric Pt electrodes of a specific surface area and a fixed distance (L) in between them. The ionic-conductivity (σ, $mScm^{-1}$) was calculated by using

$\sigma = {}^{L}/_{(Rs * A)}$ where L (cm) is the distance between the two electrodes, Rs (Ω) is the bulk resistance of the WiS-electrolyte, and A (cm^2) is the area of the platinum electrode. Hence, the calculated σ is 32.5 mScm^{-1}.

Calculation of specific energy and specific power density of battery: The specific energy and specific power densities of the Zn-graphite dual-ion battery were calculated based on the mass of graphite cathode through the following equations.

$$E\ (Whkg^{-1}) = \frac{I * V * t}{m}$$

$$P\ (Wkg^{-1}) = \frac{E}{t}$$

where I is the charging and discharging current in amperes (A), V is the average discharge voltage in volts (V), t is the discharging time in hours (h), m is the mass of graphite cathode in kg. The calculated energy and power densities of the as-presented Zn-graphite dual-ion battery are in the range of 77-35 Whkg^{-1} and 168-517 Wkg^{-1}, respectively.

Figures

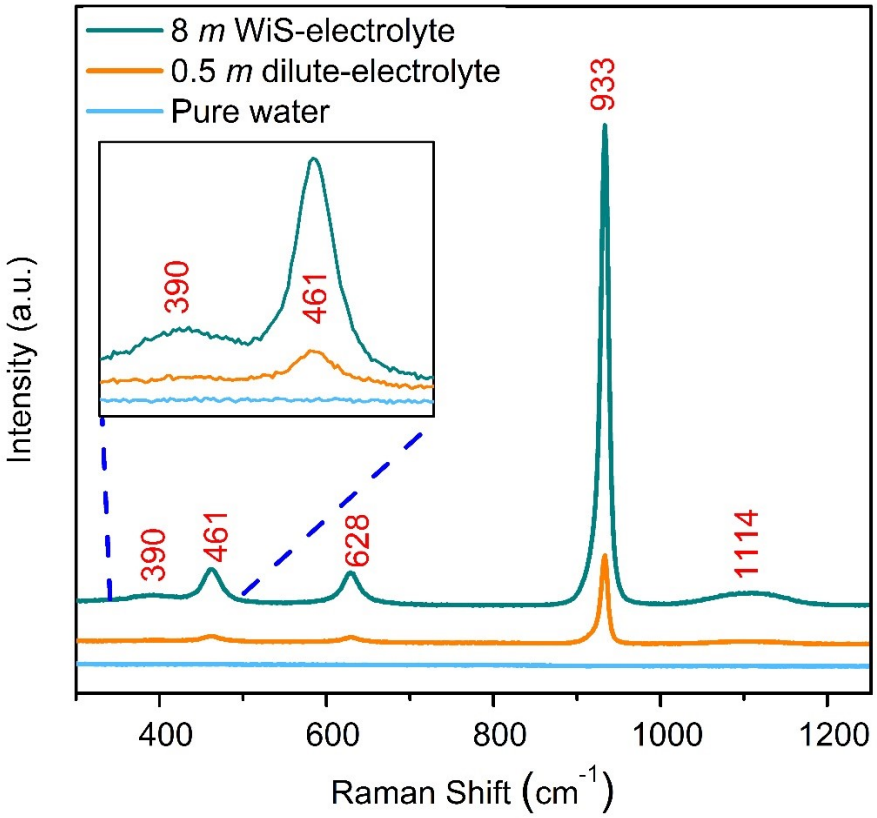

Figure S1. Raman spectra of an 8 *m* $Zn(ClO_4)_2$ WiS-electrolyte in comparison to a dilute 0.5 *m* $Zn(ClO_4)_2$ aqueous electrolyte and pure water. Peak positions are indicated for each Raman peak in wavenumbers (cm^{-1}).

Raman bands at 933 cm^{-1}, 1114 cm^{-1}, 628 cm^{-1}, and 461 cm^{-1} are associated with tetrahedral ClO_4^-, whereas the polarized band at 390 cm^{-1} is due to the Zn^{2+}-oxygen symmetric stretching mode of the $[Zn(OH_2)_6]^{2+}$ cation which is more evident in the case of the supersaturated WiS-electrolyte [1].

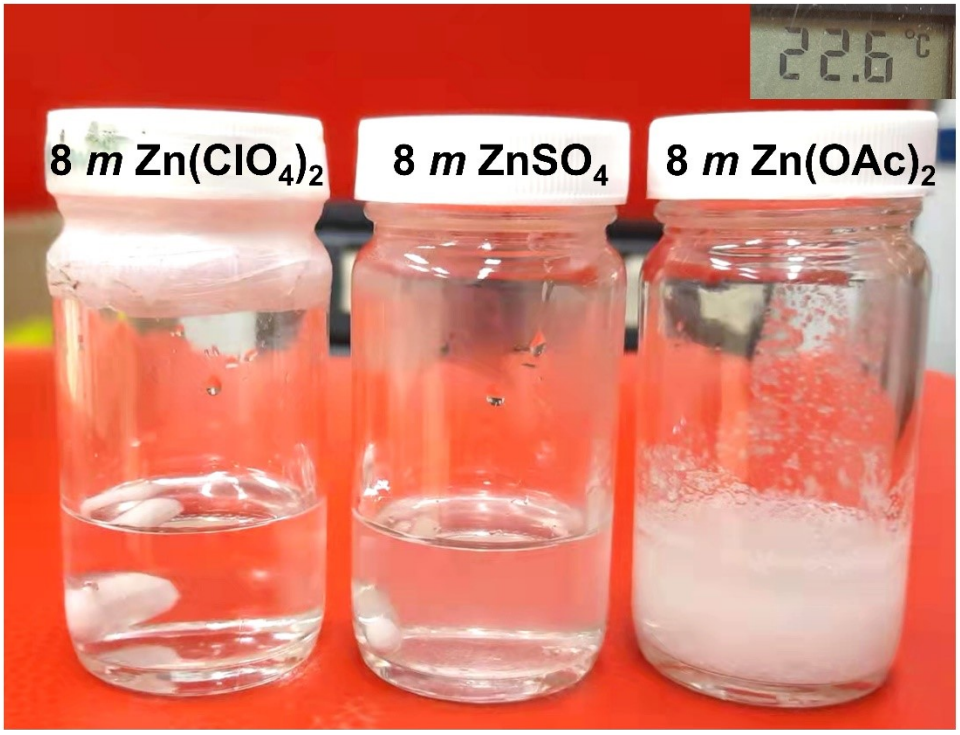

Figure S2. Physical appearance of different superconcentrated Zn-salt aqueous electrolytes at room temperature: transparent 8 *m* $Zn(ClO_4)_2$ WiS electrolyte (left), 8 *m* $ZnSO_4$ WiS electrolyte (middle), and two-phase 8 *m* $Zn(OAc)_2$ electrolyte with excess undissolved salt crystals (right).

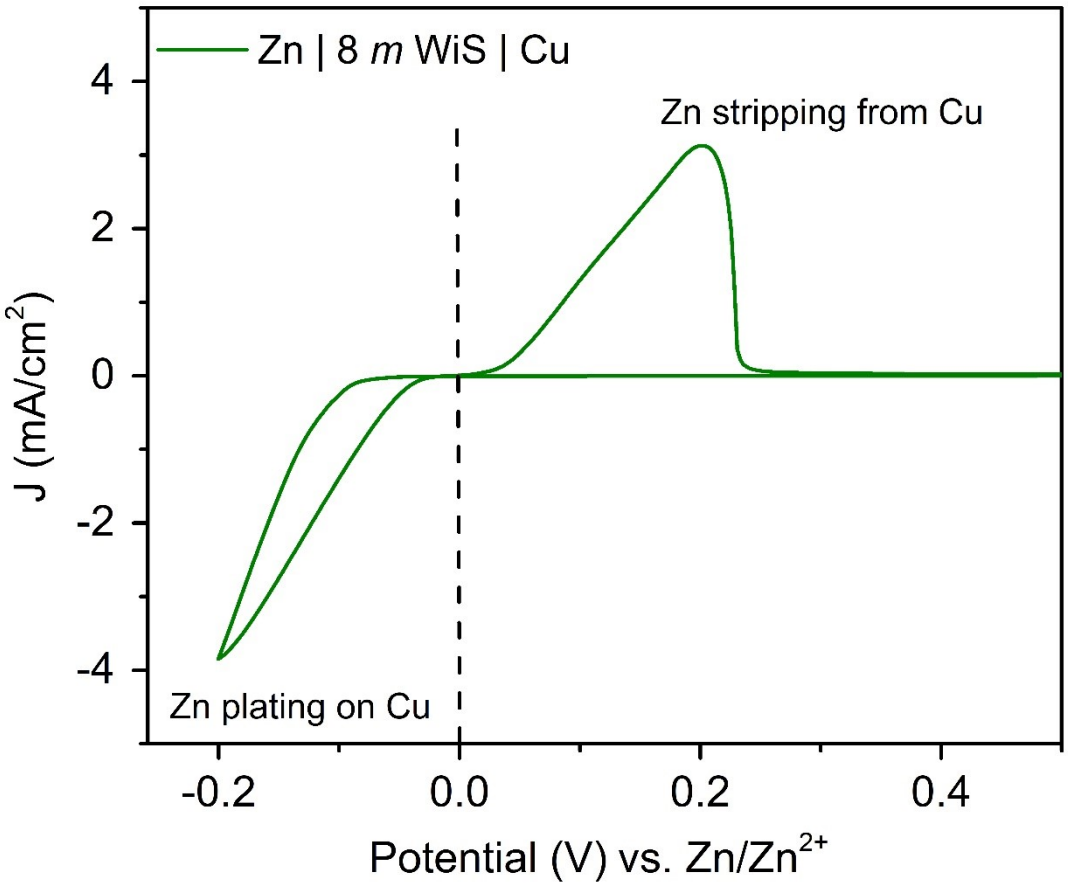

Figure S3. Cyclic voltammetry (CV) of Zn stripping/platting from an 8 *m* $Zn(ClO_4)_2$ WiS-electrolyte from/on a Cu substrate at a scan rate of 10 mVs^{-1} in a three-electrode electrochemical cell with Zn as C.E. and R.E.

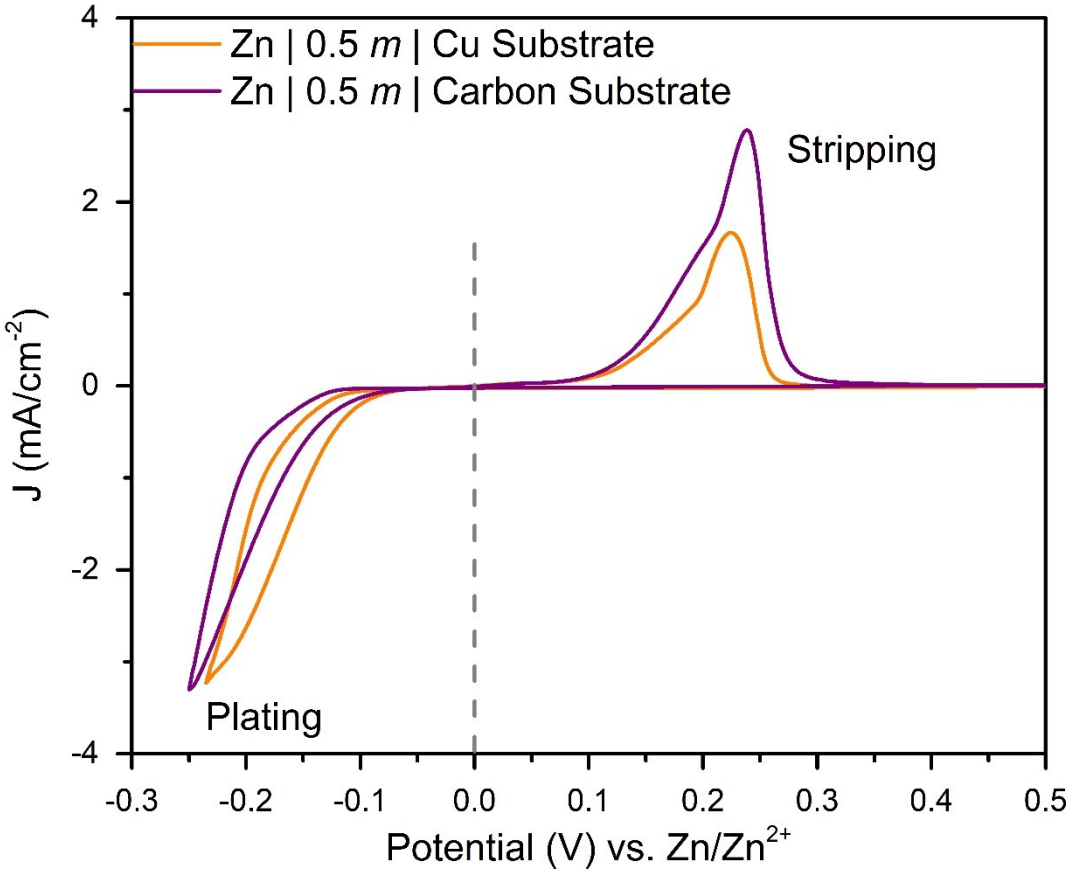

Figure S4. Cyclic voltammetry (CV) of Zn stripping/platting from a dilute 0.5 *m* $Zn(ClO_4)_2$ electrolyte from/on the Cu and carbon (C120 Toray) substrate at a scan rate of 10 mVs^{-1} in a two-electrode electrochemical cell with Zn as C.E. and R.E

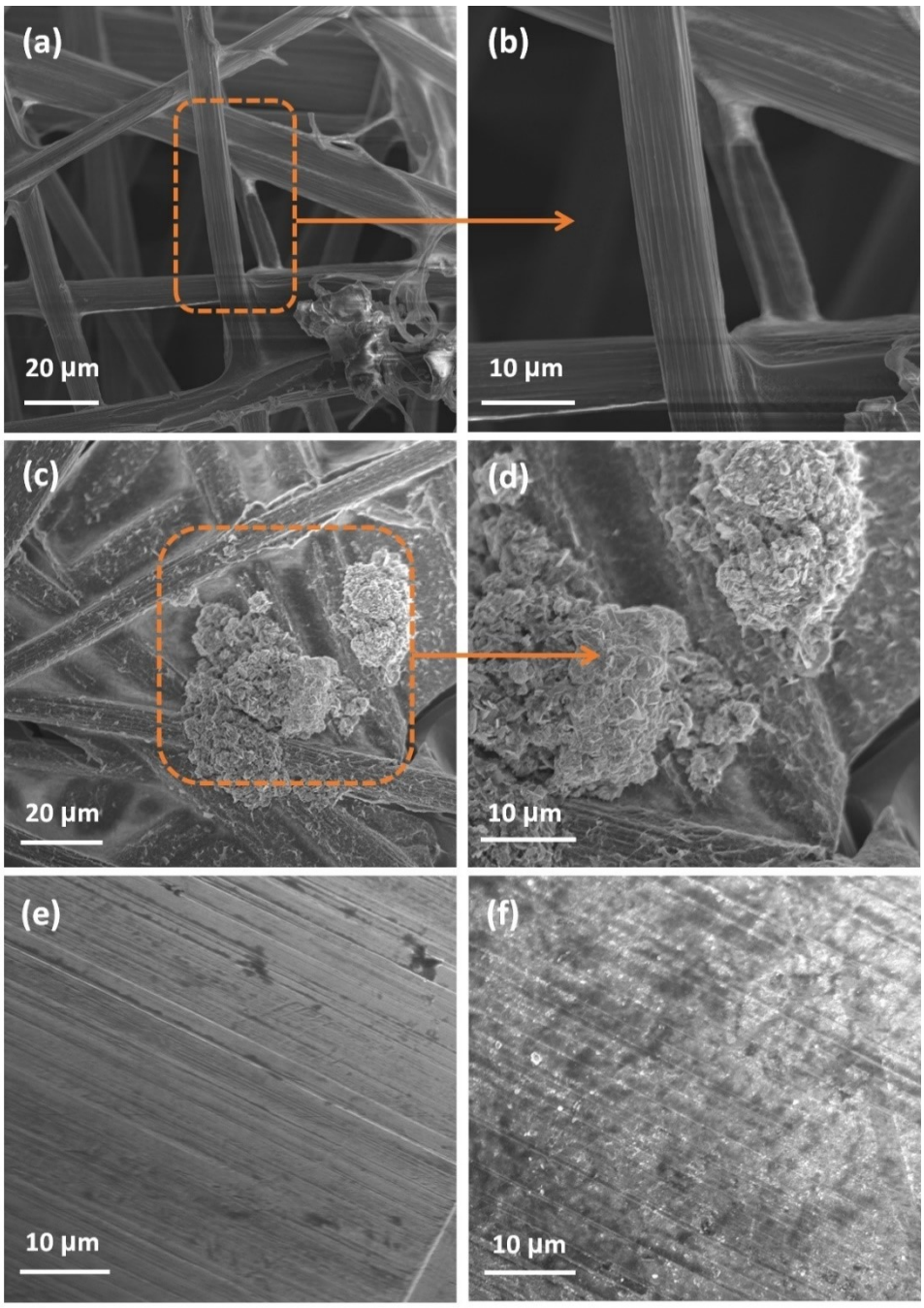

Figure S5. SEM images showing morphology of different substrates before and after Zn deposition from a dilute 0.5 *m* $Zn(ClO_4)_2$ electrolyte: carbon (C120 Toray) substrate, pristine (a) & (b), and after Zn deposition (c) & (d); Cu substrate, pristine (e), and after deposition (f).

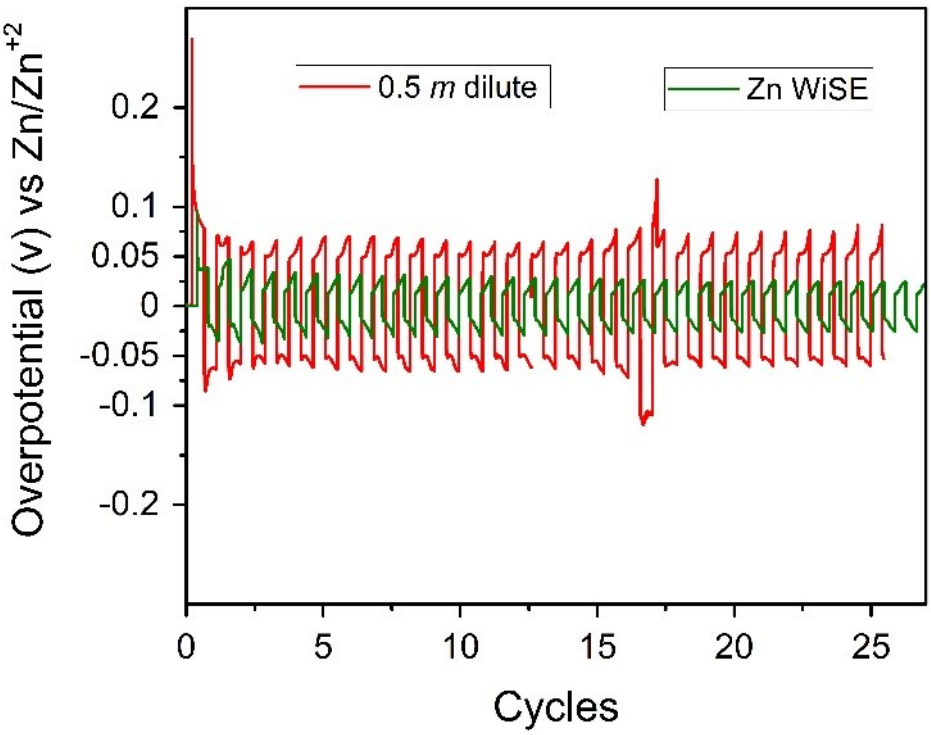

Figure S6. Comparison of overpotential of stripping/plating analysis of Zn||Zn cell using a diluted 0.5 *m* $Zn(ClO_4)_2$ aqueous electrolyte and 8 *m* $Zn(ClO_4)_2$ WiS-electrolyte.

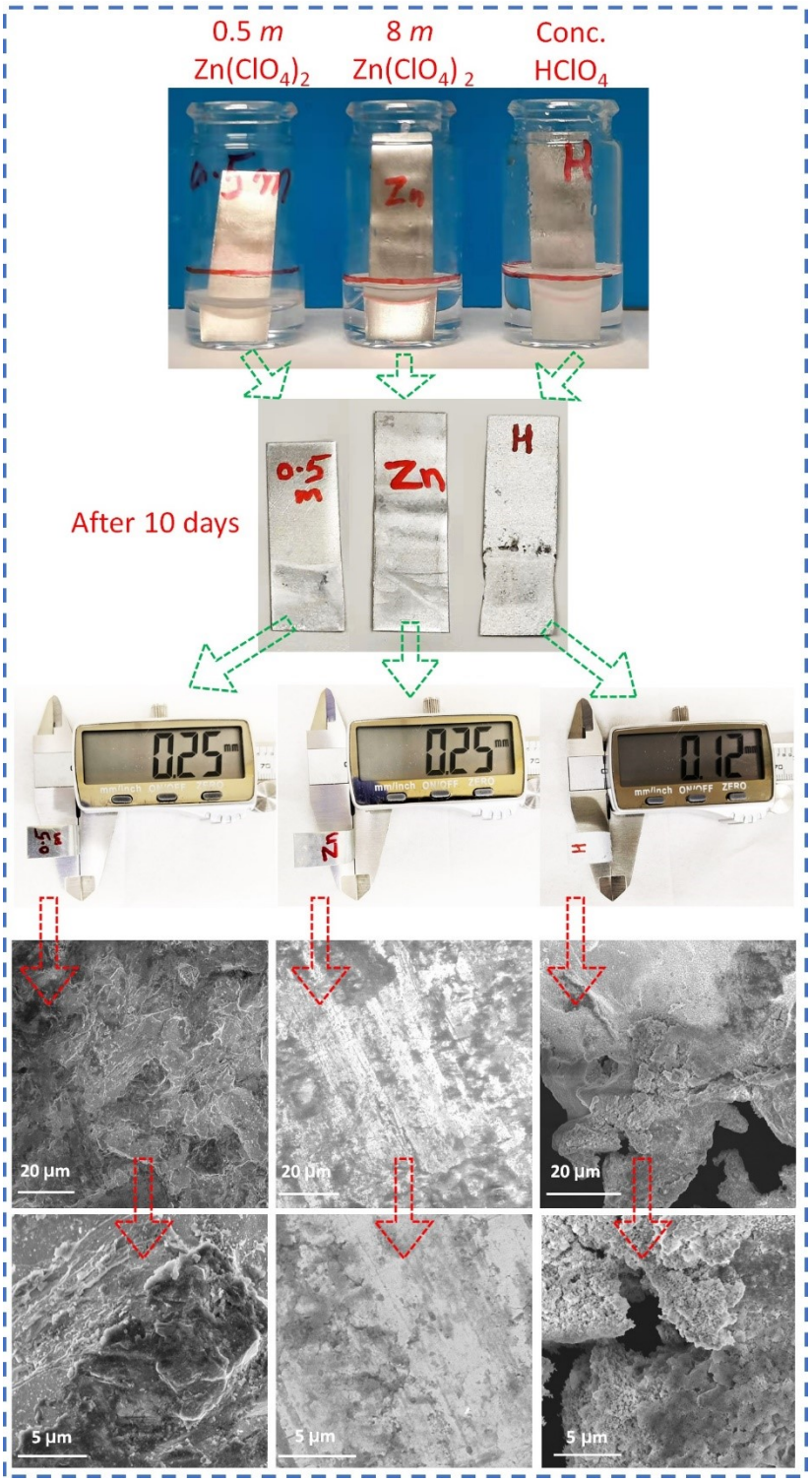

Figure S7. Zn self-dissolution and corrosion test in a dilute 0.5 *m* $Zn(ClO_4)_2$ aqueous electrolyte (pH~5.0), 8 *m* $Zn(ClO_4)_2$ WiS-electrolyte (pH~1.0), and 70.5 % $HClO_4$ acid (pH~1.0): Zn metal strips after immersion of 10 days in 0.5 m=$Zn(ClO_4)_2$ dilute electrolyte, Zn=$Zn(ClO_4)_2$ WiS-electrolyte and H=$HClO_4$ acid and their corresponding thicknesses and SEM images. Pristine Zn metal thickness: 0.25 mm. The SEM images of Zn foil immersed into WiS-electrolyte are the same as of pristine Zn metal, but the Zn foil immersed into the dilute electrolyte and $HClO_4$ undergone spontaneous corrosion and self-dissolution processes as SEM imaged show a modified surface morphology.

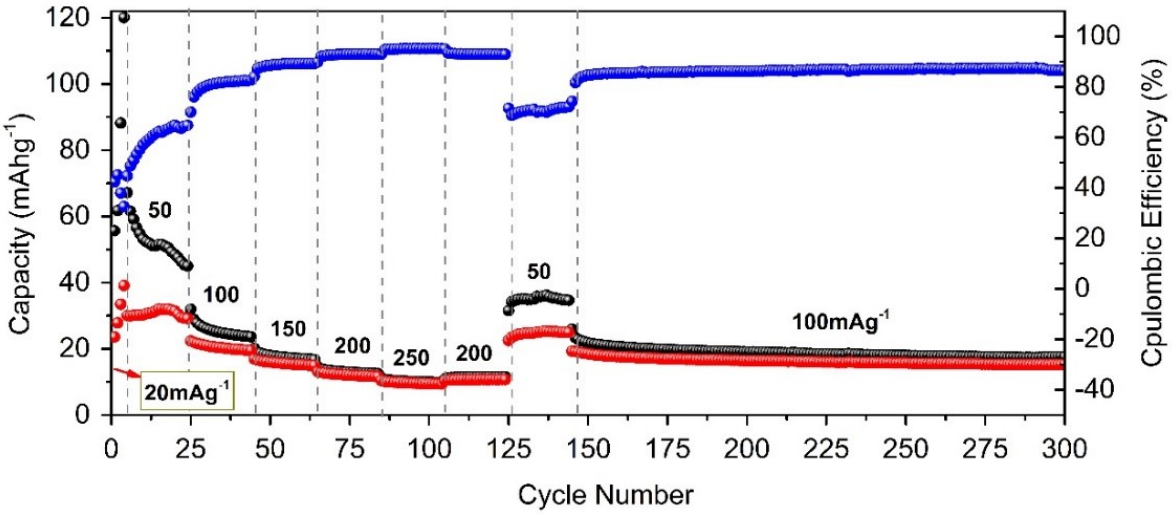

Figure S8. Rate-capability and cycling performance of a Zn-graphite dual-ion battery at the cut-off voltage of 2.45 V vs. Zn/Zn^{2+}.

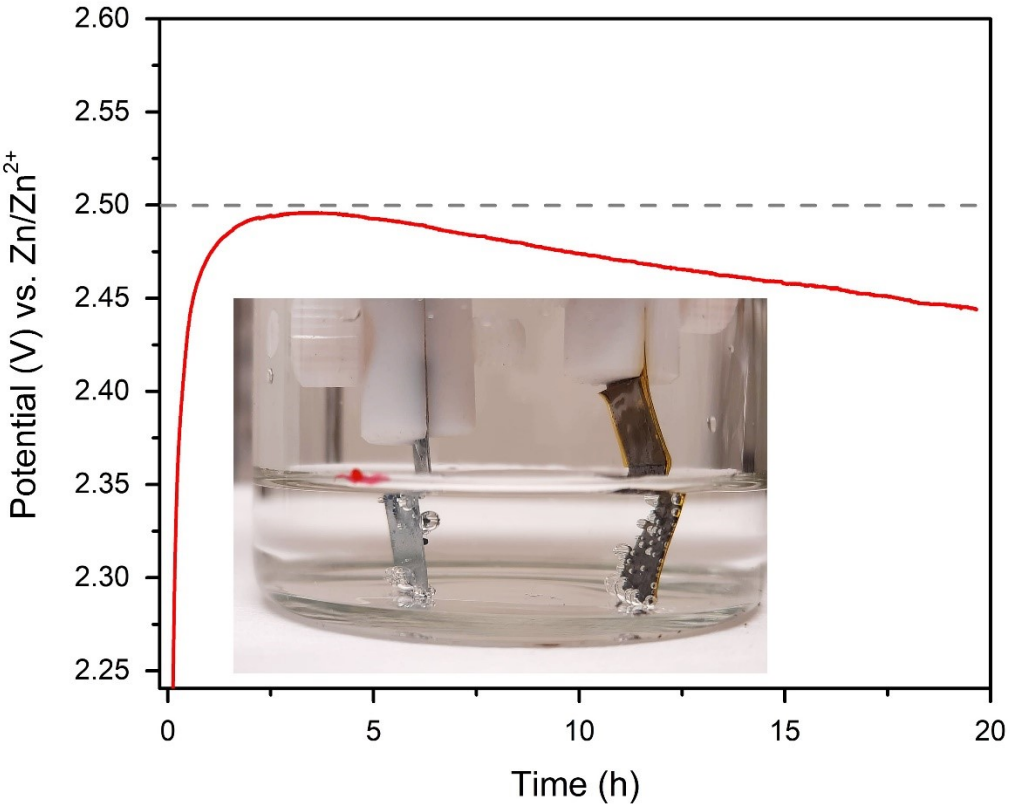

Figure S9. Electrochemical performance of a Zn-graphite dual-ion battery utilizing dilute (0.5 *m*) $Zn(ClO_4)_2$ aqueous electrolyte, inset showing gas evolution (electrolyte decomposition) at a high charging potential.

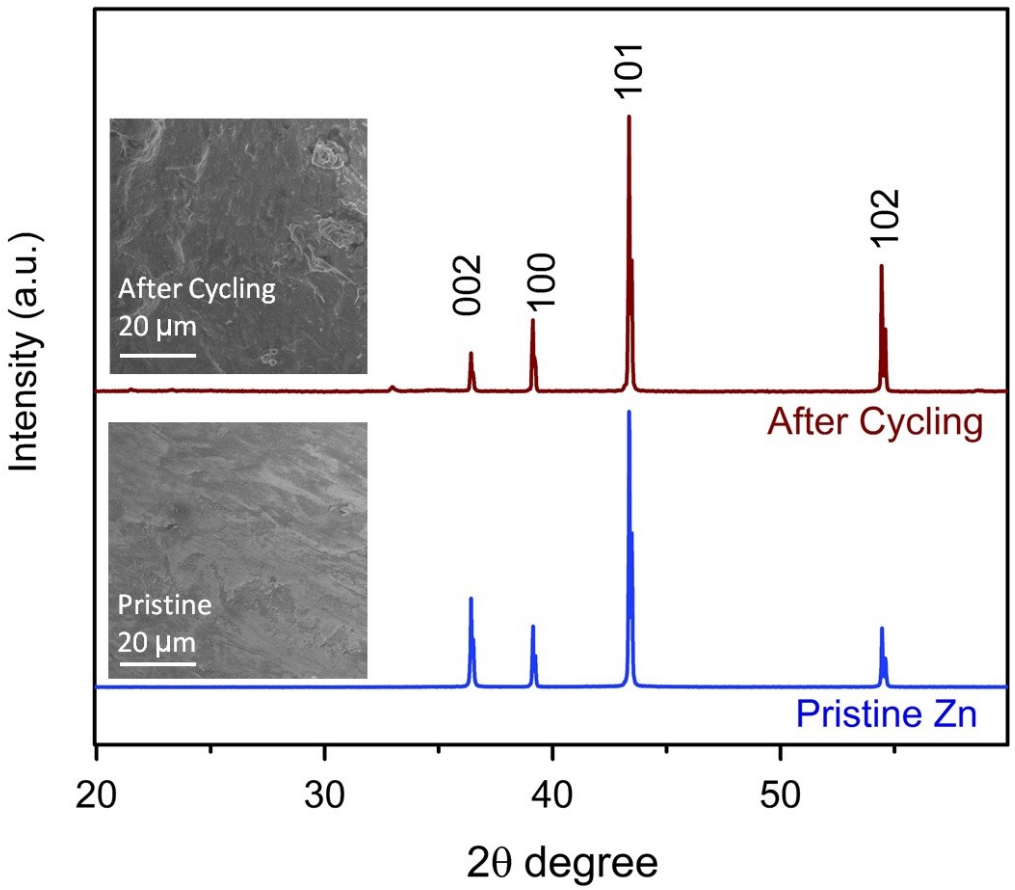

Figure S10. XRD and corresponding SEM of pristine and cycled Zn anodes.

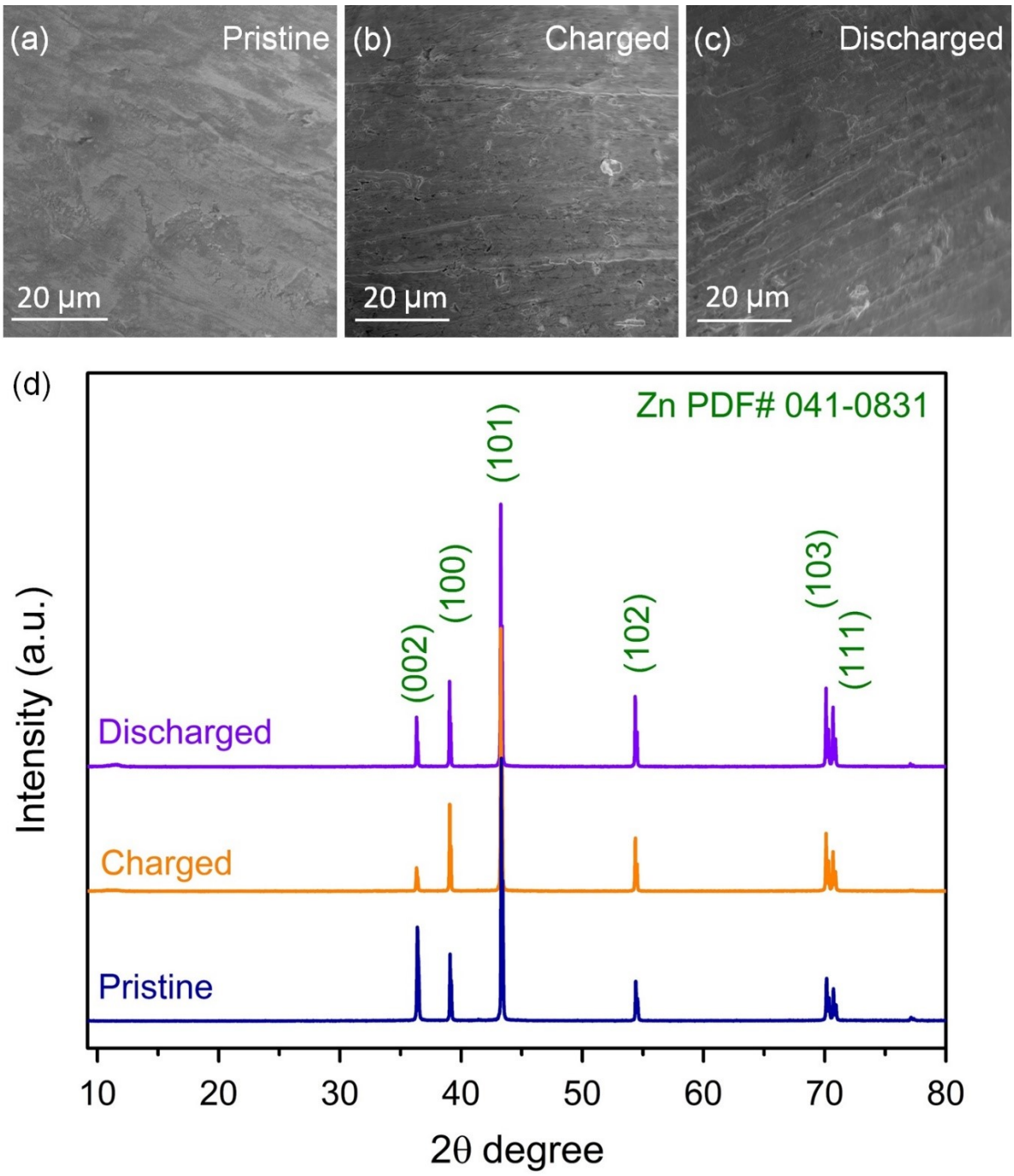

Figures S11. SEM images of pristine (a), charged (b), and discharged (c) Zn anodes after the 30th cycle; corresponding XRD of the samples (d).

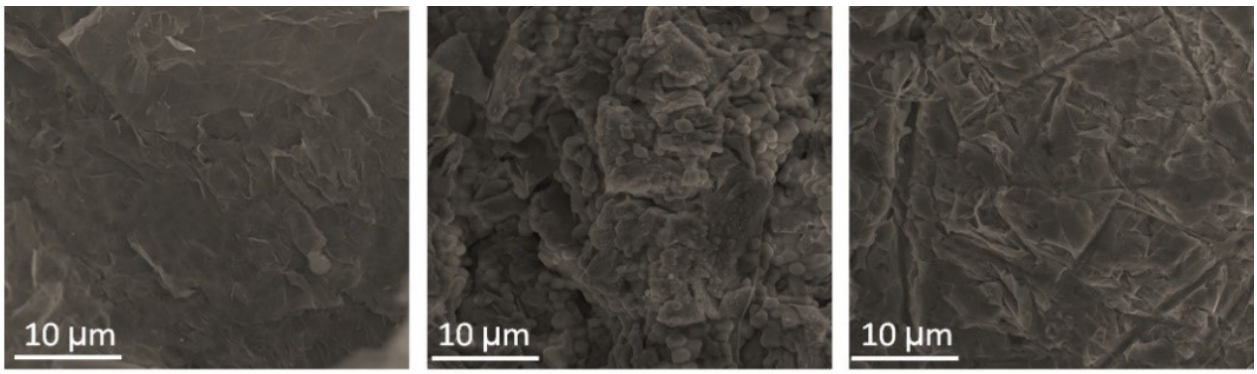

Figure S12. SEM images of freshly-modified (left), fully charged (center), and fully discharged carbon paper electrodes (right).

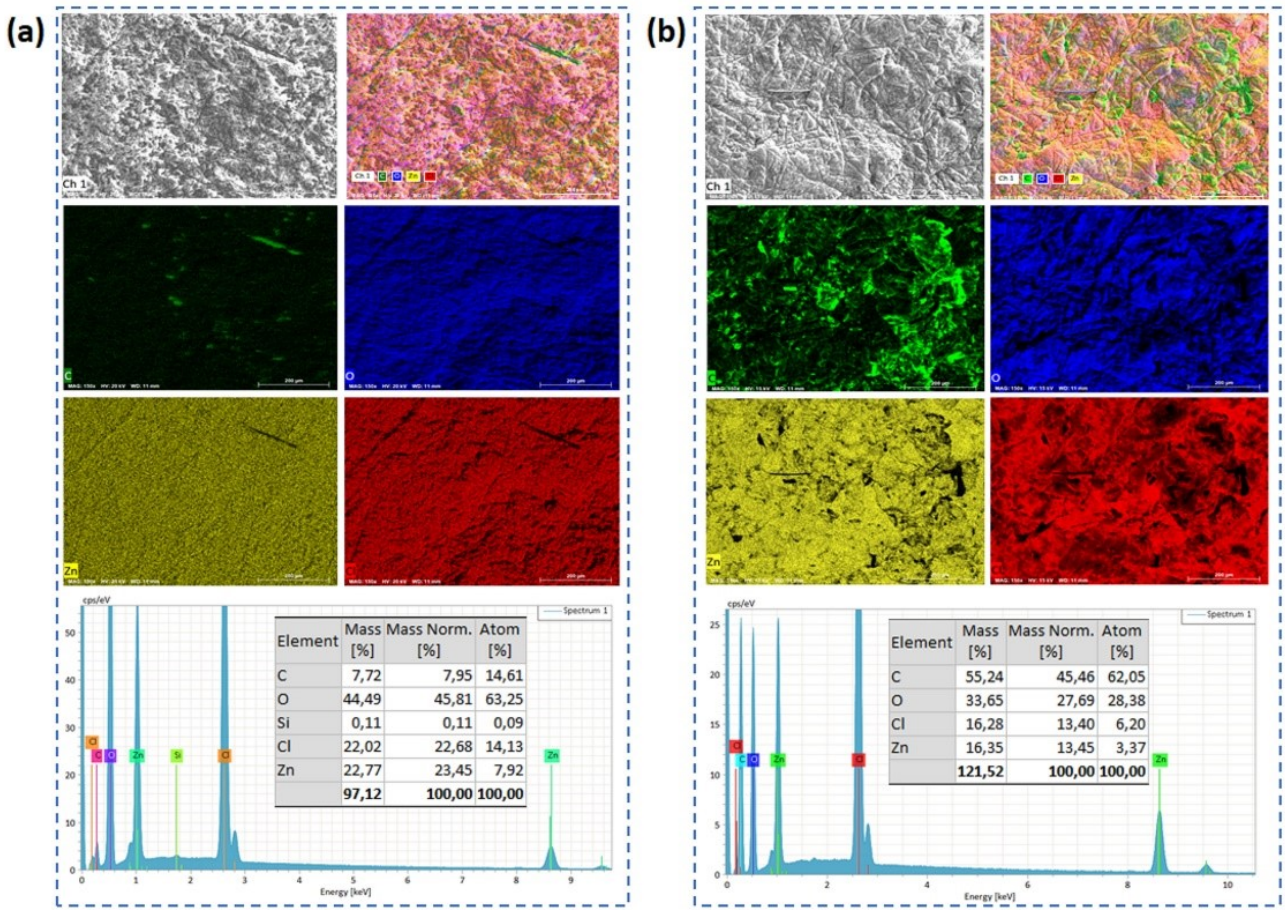

Figure S13. Energy-dispersive X-Ray spectroscopy (EDS) analysis of charged (a), and discharged GP cathodes (b) along with elemental mapping (scale bar 200 µm), EDS spectrum, and elemental compositions.

Table S1 A comparison of the as reported Li^+ -free and uni-salt based WiS-electrolyte (8 *m* $Zn(ClO_4)_2$) with previously reported WiS-electrolytes for Zn-ion and Zn-graphite dual-ion batteries is presented. As comparison metrics, the ionic conductivities, electrochemical stability window (ESW), and mean-discharge voltage of the reported cell systems in WiS-electrolytes are presented.

Type of WiS electrolyte	Ionic Conductivity (mS/cm²)	ESW (V)	Cell System Cathode	Mean Voltage (V)	Ref.
8 *m* $Zn(ClO_4)_2$	**32.5**	**2.80**	**Zn/G**	**1.95**	**This Work**
21 *m* LiTFSI + 3 *m* $ZnTfO_2$	7	2.6	Zn/G	1.7	[2]
20 *m* NaFSI + 0.5 *m* $Zn(TFSI)_2$	-	2.7	Zn/G	2.25	[3]
1 *m* $Zn(ClO_4)_2$+10 *m* $LiClO_4$	5.31	3	$Zn/LiMn_2O_4$	~1.7	[4]
0.5 *m* $Zn(ClO_4)_2$ + 18 *m* $NaClO_4$	98.5	-	$Zn/Na_2V_6O_{16}{\cdot}nH_2O$	0.8	[5]
30 *m* $ZnCl_2$	2	2.3	-	-	[6]
30 *m* $ZnCl_2$	-	-	$Zn_3[Fe(CN)_6]_2$ /Fc/C	0.95	[7]
21 *m* LiTFSI+0.5 *m* $ZnSO_4$	-	-	$Zn/LiMn_{0.8}Fe_{0.2}PO_4$	1.8	[8]
15 *m* $ZnCl_2$ +1.0 *m* LiCl	-	2.4	$Zn/LiFePO_4$	1.35	[9]
30 *m* KAC + 3 *m* LiAc + 3 *m* $ZnAc_2$	6.5	~2.2	$Zn/LiFePO_4$	1.35	[10]
21 *m* LiTFSI + 1 *m* $Zn(CF_3SO_3)_2$	-	-	Zn/V_2O_5	1.4	[11]
21 *m* LiTFSI + 3 *m* $ZnOTf_2$ + 10 wt. % of PVA	~2.1	~2.6	Zn/V_2O_5	1	[12]

Table S2. The chemical composition of elements in pristine, charged, and discharged GP by XPS.

Sample	Zn (At.%)	Cl (At.%)	C (At.%)	O (At.%)	Zn/C	Cl/C	O/C
Pristine GP	0.0	0.0	98.4	1.6	0	0	0.02
Charged GP	36.6	12.2	13.7	37.5	2.67	0.89	2.73
Discharge	38.5	10.8	20.2	30.5	1.90	0.53	1.50

References

1. W. W. Rudolph and C. C. Pye, *J. Sol. Chem.*, 1999, **28**, 1045-1070.
2. H. Zhang, X. Liu, B. Qin and S. Passerini, *J. Power Sources*, 2020, **449**, 227594.
3. I. A. Rodríguez-Pérez, L. Zhang, J. M. Wrogemann, D. M. Driscoll, M. L. Sushko, K. S. Han, J. L. Fulton, M. H. Engelhard, M. Balasubramanian, V. V. Viswanathan, V. Murugesan, X. Li, D. Reed, V. Sprenkle, M. Winter and T. Placke, *Adv. Energy Mater.*, 2020, **10**, 2001256.
4. S. Chen, R. Lan, J. Humphreys and S. Tao, *ACS Appl. Energy Mater.*, 2020, **3**, 2526-2536.
5. Y. Zhu, J. Yin, X. Zheng, A.-H. Emwas, Y. Lei, O. F. Mohammed, Y. Cui and H. N. Alshareef, *Energy Environ. Sci.*, 2021, **14**, 4463-4473.
6. C. Zhang, J. Holoubek, X. Wu, A. Daniyar, L. Zhu, C. Chen, D. P. Leonard, I. A. Rodriguez-Perez, J. X. Jiang, C. Fang and X. Ji, *Chem. Commun*, 2018, **54**, 14097-14099.
7. X. Wu, Y. Xu, C. Zhang, D. P. Leonard, A. Markir, J. Lu and X. Ji, *J. Am. Chem. Soc.*, 2019, **141**, 6338-6344.
8. J. Zhao, Y. Li, X. Peng, S. Dong, J. Ma, G. Cui and L. Chen, *Electrochem. Commun.*, 2016, **69**, 6-10.
9. X. Zhong, F. Wang, Y. Ding, L. Duan, F. Shi and C. Wang, *J. Electroanal. Chem.*, 2020, **867**, 114193.
10. J. Han, A. Mariani, A. Varzi and S. Passerini, *J. Power Sources*, 2021, **485**, 229329.
11. P. Hu, M. Yan, T. Zhu, X. Wang, X. Wei, J. Li, L. Zhou, Z. Li, L. Chen and L. Mai, *ACS Appl. Mater. Interfaces*, 2017, **9**, 42717-42722.
12. H. Zhang, X. Liu, H. Li, B. Qin and S. Passerini, *ACS Appl. Mater. Interfaces*, 2020, **12**, 15305-15312.